Synchronous oscillations in the cerebral cortex

P. A. Robinson,[1,*] J. J. Wright,[2,†] and C. J. Rennie[1,3,‡]
[1]*School of Physics, University of Sydney, New South Wales 2006, Australia*
[2]*Mental Health Research Institute, Parkville, Victoria 3052, Australia*
[3]*Department of Medical Physics and Cognitive Neuroscience Unit, Westmead Hospital, Westmead, New South Wales 2145, Australia*
(Received 27 March 1997; revised manuscript received 19 September 1997)

The dynamics of a cortex driven by a finite number of white-noise point sources is studied using a recently developed wave-equation formulation. Green's functions, power spectra, fluctuation levels, and two-point correlation functions are computed analytically and numerically. It is shown that a range of observed properties of so-called synchronous oscillations in the cerebral cortex can be correctly reproduced using the wave equation that involves only excitatory interactions between neurons. In particular, the observed existence of a maximal correlation at zero temporal lag between spatially separated points is reproduced and explained for a cortex driven by two white-noise sources. [S1063-651X(98)03904-X]

PACS number(s): 87.22.Jb, 87.22.As, 87.10.+e

I. INTRODUCTION

A long-standing puzzle in neurophysiology is the so-called *binding problem*, which may be stated as follows: Among the many concurrent patterns of neuronal activity present simultaneously in the billions of neurons in the brain, how are related aspects of a single stimulus bound together? For example, how are the disparate features of a face, each analyzed by specific cerebral areas that receive visual input and respond specifically to movement, angles, color, etc., associated and seldom confused with incidental aspects of the background, despite complex concurrent changes in the visual stimulus? Recent findings in neurophysiology indicate that the solution of this problem may lie in the brain's use of a phenomenon termed *synchronous oscillation* to correlate spatially separated responses to a stimulus. The main purpose of this paper is to apply the recently developed wave-equation formulation of cortical dynamics [1] to elucidate this phenomenon.

It has been shown that clusters of neurons at simultaneously stimulated sites in the cortex and elsewhere in the brain can exhibit synchronous oscillations of neural firing rates over distances comparable to the size of the cortex and that this synchrony typically appears in circumstances when the stimulus properties are such that the features of the stimulus demand binding if a perceptual whole is to be created [2–4]. In this context synchronous oscillations are defined to be oscillations for which the temporal cross correlation between signals at different locations exhibits a maximum at zero lag; we will also call such oscillations *zero-lag* oscillations on occasion.

In a recent review [5] findings were summarized that showed that synchrony appears at multiple scales, from small pools of locally connected neurons to sites on opposite sides of the brain. Both structural connectivity (e.g., by cortico-cortical axonal fibers) and functional dynamic state (e.g., by level of activation of cortical sites by inputs from subcortical sites [6]) partially determine which neuronal pools synchronize with each other. Relative lags between stimulated sites can be more complicated near the site of input: Some cells in the field of input can lead others nearby by a few milliseconds, particularly if the leading cells are particularly precisely responsive to the features of the stimulus; yet apparently precise synchrony appears between more distant sites and across most cells in the local population [7].

The mechanism(s) via which the synchronous oscillation is generated is a subject of controversy and it is now fairly widely accepted that multiple mechanisms may be involved [8]. In most instances results cannot be explained by concurrent synchronous inputs to the separated sites, although this sometimes plays a role [9,10]. A variety of other experimental and theoretical approaches have been made to the problem. These include the recognition that limit cycle oscillators representing single neurons can mutually entrain to form independent synchronized clusters [11,12]. Simulations also indicate that local lateral inhibition might entrain synchrony [13] and that nonoscillating interlocking chains of neurons (so-called *synfire chains*) can shift phase into synchrony [14]. Simulations of intercellular interactions in the hippocampus, which model excitatory and inhibitory neuronal interactions via specific chemical neurotransmitters in considerable detail, were found to account for both synchrony and specific patterns of firing as seen in in-vitro slices of this region of the brain [15]. However, these results also depend primarily on local interactions among inhibitory cells and encounter some difficulty in explaining the ubiquity of long-range synchrony mediated by excitatory connections.

All these attempts at elucidation and explanation have tended to concentrate upon interactions between specific cells, considered as interacting discretely with each other, while ignoring the fact of the embedding of these cells in a continuum of intercellular connections. These considerations raise the possibility that synchronous oscillation might be a continuum property of large fields of interconnected cells and might thus be best accounted for by continuum-field models of neuronal interactions. Such models have been developed primarily to account for traveling-wave properties,

*Electronic address: robinson@physics.usyd.edu.au
†Electronic address: jjw@cortex.mhri.edu.au
‡Electronic address: rennie@physics.usyd.edu.au

and electrocortical activity more generally, which is usually recorded from the scalp as an electroencephalogram.

Prominent among models treating the properties of the extended coupled neuronal field are those of Freeman [16] and Nunez [17]. Recently we proposed a model based on similar assumptions, incorporating locally coupled excitatory and inhibitory neuronal populations, long-range excitatory connections, dendritic integration, and axonal time delays [1,18,19]. The resulting equations describe the spatial and temporal properties of a uniform cortex in the continuum approximation and permit simulations on any scale greater than that of the inhibitory neurons (a few tenths of a millimeter). Using these numerical simulations, it has been demonstrated recently that fields of zero-lag synchrony that reproduce general features of the experimental data can be readily generated [20]. The fields of zero-lag synchrony appear as part of a larger field of lag-correlated (traveling-wave) activity and do not depend upon synchrony of inputs, nonlinearity of the simulated neurons, or interactions between excitatory and inhibitory cells: Purely excitatory interactions are sufficient.

Recently, we proposed a nonlinear model of cortical dynamics [1], similar in physical basis to versions of the dynamical equations introduced earlier [18,19], but replacing their formulation in terms of Green's functions by a wave-equation approach [1]. This model was not identical to the previous ones, but incorporated the same neurophysics to a similar degree of approximation. This model allowed us to find cortical steady states and analyze their stability and to study the propagation and stability of small-amplitude cortical waves. In the present paper we use it to calculate analytically the response of the cortex to a finite number of point sources of stimulation. The results are used to show that synchronous oscillations arise naturally in the cortex and can be explained simply in terms of propagating waves.

The structure of this paper is as follows. In Sec. II we briefly review the wave-equation model and write down the linearized wave equation. We then derive the Green's function for propagating cortical waves and use it to calculate correlation functions, levels and times of maximal correlations, and spectra of fluctuations excited by a finite number of point sources. In Sec. III we evaluate these expressions numerically for some representative cases and compare the results with direct solution of the full set of nonlinear cortical-dynamics equations. Comparisons with experimental results for synchronous oscillations are also discussed in Sec. IV.

II. THEORY

In this section we first outline the main relevant results of our recently developed wave-equation formulation of cortical dynamics [1]. These results are then applied to derive the Green's function of propagating cortical disturbances, and the two-point correlation function and power spectrum of cortical fluctuations driven by a finite number of point sources. In all cases we restrict attention to regimes in which only stable waves exist [1]; cortical instabilities are not considered.

A. Dynamical equations

In a previous paper [1] we developed a set of nonlinear equations for cortical dynamics in the continuum limit. These equations incorporated excitatory and inhibitory neurons, dendritic integration of inputs to a given neuron, finite axonal propagation velocities, and the nonlinear relationship between inputs to a neuron and its firing rate.

The first of the central equations of our model is

$$Q_{e,i}(\mathbf{r},t)=\frac{1}{1+e^{-C[V_{e,i}(\mathbf{r},t)-V_0]}}, \tag{1}$$

which relates the mean firing rate $Q_{e,i}(\mathbf{r},t)$ of neurons (the *pulse density* in neurophysiological terminology) to the applied potential $V_{e,i}(\mathbf{r},t)$, where e and i denote the excitatory and inhibitory populations, and C and V_0 are constants or order unity. Potentials are measured in units of the standard deviation of the distribution of neuronal firing thresholds.

The potential $V_{e,i}(\mathbf{r},t)$ at the point where conversion to neuronal pulses takes place results after inputs have been summed and filtered through the dendrites. A good approximation to $V_{e,i}(\mathbf{r},t)$ is given by

$$V_{e,i}(\mathbf{r},t)=g\frac{\alpha\beta}{\beta-\alpha}[U_{e,i}(\mathbf{r},t)-W_{e,i}(\mathbf{r},t)], \tag{2}$$

$$\frac{dU_{e,i}(\mathbf{r},t)}{dt}=Q_{ae,ai}(\mathbf{r},t)-\alpha U_{e,i}(\mathbf{r},t), \tag{3}$$

$$\frac{dW_{e,i}(\mathbf{r},t)}{dt}=Q_{ae,ai}(\mathbf{r},t)-\beta W_{e,i}(\mathbf{r},t), \tag{4}$$

where $Q_{ae,ai}(\mathbf{r},t)$ represent arrival rates of input pulses at the dendrites, g is a dendritic gain factor, and α and β are constants parametrizing the dendritic response to an impulse. In effect, diffusion during dendritic propagation smears out the temporal response and the dendritic tree acts as a low-pass filter.

Outgoing pulses from each neuron propagate along its axon and axonal tree at a characteristic velocity v. Assuming an isotropic distribution of axons whose ranges have an approximately exponential distribution (see Ref. [1] for details), this propagation can be modeled by a wave equation for the corresponding potentials $\phi_{e,i}(\mathbf{r},t)$:

$$\left(\frac{\partial^2}{\partial t^2}+2\gamma_{e,i}\frac{\partial}{\partial t}+\gamma_{e,i}^2-v^2\nabla^2\right)\phi_{e,i}(\mathbf{r},t)=\gamma_{e,i}^2Q_{e,i}(\mathbf{r},t), \tag{5}$$

where $\gamma_{e,i}=v/r_{e,i}$ and $r_{e,i}$ are the characteristic ranges of the axons [1].

The incident potentials $Q_{ae,ai}(\mathbf{r},t)$ at a particular location comprise contributions from the wave potentials $\phi_{e,i}$ and inputs external to the cortex. These inputs are usually split into two components: a uniform mean *nonspecific* excitation Q_{ns} that results from the total of inputs from noncortical structures in the brain and a *specific* excitation $Q_s(\mathbf{r},t)$ associated with the stimulus under investigation. Robinson *et al.* [1] defined Q_{ns} to be constant in time and space, while

$Q_s(\mathbf{r},t)$ has zero spatial and temporal averages, leading to the final underlying equations of our model:

$$Q_{ae}(\mathbf{r},t)=M_eQ_s(\mathbf{r},t)+\mu_eQ_{ns}+a_{ee}\phi_e(\mathbf{r},t)-a_{ei}\phi_i(\mathbf{r},t), \tag{6}$$

$$Q_{ai}(\mathbf{r},t)=M_iQ_s(\mathbf{r},t)+\mu_iQ_{ns}+a_{ie}\phi_e(\mathbf{r},t)-a_{ii}\phi_i(\mathbf{r},t). \tag{7}$$

Here the constants $M_{e,i}$ determine the strength of coupling of specific inputs to excitatory and inhibitory neurons, $\mu_{e,i}$ are the coupling strengths for nonspecific impulses (i.e., the relevant fractional synaptic densities), and the coefficients a_{mn} are the synaptic densities associated with excitatory and inhibitory inputs to excitatory and inhibitory neurons.

B. Wave equation

Robinson *et al.* [1] showed that Eqs. (1)–(7) have a stable low-Q_e fixed point provided Q_{ns} is not too large. Linearizing the system around this fixed point, they wrote down an approximate wave equation for the excitatory wave potential ϕ_e alone, from which all other fields could be derived in the linear limit. In Fourier space, this equation is

$$[D_e(\mathbf{k},\omega)-F_e(\omega)a_{ee}]\phi_e(\mathbf{k},\omega)=F_e(\omega)M_eQ_s(\mathbf{k},\omega), \tag{8}$$

where the cortex is driven by a specific input $Q_s(\mathbf{k},\omega)$, $\mathbf{k}$ is the wave vector, ω is the angular frequency,

$$F_e(\omega)=g\rho_e\gamma_e^2L(\omega), \tag{9}$$

$$L(\omega)=\frac{\alpha\beta}{(\alpha-i\omega)(\beta-i\omega)}, \tag{10}$$

$$D_e(\mathbf{k},\omega)=(\gamma_e-i\omega)^2+k^2v^2, \tag{11}$$

$$\rho_e=CQ_e^{(0)}[1-Q_e^{(0)}], \tag{12}$$

and $Q_e^{(0)}$ is the equilibrium pulse density.

For freely propagating waves, Eq. (8) yields the dispersion equation [1]

$$(\alpha-i\omega)(\beta-i\omega)D_e(\mathbf{k},\omega)-\alpha\beta\gamma_e^2G=0 \tag{13}$$

for $Q_s=0$, with

$$G=g\rho_ea_{ee}. \tag{14}$$

Equation (13) implies that only the excitatory field need be followed for low $Q_e^{(0)}$, with only excitatory quantities entering its dispersion equation. This is reasonable given the preponderance of excitatory connections between neurons. Robinson *et al.* [1] showed that this yields a good approximation to the dispersive properties of the model medium provided the wavelengths of the waves are much greater than a few tenths of a millimeter. This is not a significant constraint in practice because typical wavelengths are a few centimeters in the human cortex. They also showed that waves are stable for $G<1$, which will be assumed in what follows here. Wright [20] showed numerically that inhibitory-excitatory interactions can play a role in determining the so-called gamma-band (30–80 Hz) spectrum in a strongly stimulated cortex, but we will not consider this problem here. We have recomputed most of the results of this paper with the inclusion of inhibition, finding only negligible changes for typical parameters, so we omit these refinements for simplicity.

C. Green's function

We are interested in calculating the correlation between $\phi_e(\mathbf{r},t)$ and $\phi_e(\mathbf{r}',t+\tau)$ as a function of $\mathbf{r}$, $\mathbf{r}'$, and τ, a quantity that is experimentally measured. Hence we first wish to calculate $G(r,\omega)$ to determine the effect of a point source of frequency ω at a range r. Later we will integrate this quantity over a frequency spectrum and sum over point sources to obtain the correlation function in question.

In Fourier space, the Green's function for the wave equation (8) is

$$G(\mathbf{k},\omega)=\frac{L(\omega)\gamma_e^2g\rho_e}{k^2v^2+(\gamma_e-i\omega)^2-L(\omega)\gamma_e^2G}. \tag{15}$$

Using this relationship we can write

$$G(r,\omega)=\frac{L(\omega)\gamma_e^2G}{a_{ee}v^2}\int\frac{d^2\mathbf{k}}{(2\pi)^2}\frac{e^{i\mathbf{k}\cdot\mathbf{r}}}{k^2+q(\omega)^2} \tag{16}$$

$$=\frac{L(\omega)\gamma_e^2G}{a_{ee}v^2}\int_0^\infty\frac{dk\ k}{2\pi}\int_0^{2\pi}\frac{d\theta}{2\pi}\frac{e^{ikr\cos\theta}}{k^2+q(\omega)^2} \tag{17}$$

$$=\frac{L(\omega)\gamma_e^2G}{2\pi a_{ee}v^2}\int_0^\infty dk\frac{kJ_0(kr)}{k^2+q(\omega)^2} \tag{18}$$

$$=\frac{L(\omega)\gamma_e^2G}{2\pi a_{ee}v^2}K_0[q(\omega)r] \tag{19}$$

$$q(\omega)=\frac{1}{v}[(\gamma_e-i\omega)^2-L(\omega)\gamma_e^2G]^{1/2}, \tag{20}$$

where J_0 and K_0 denote Bessel and Macdonald functions, respectively. Note that the root chosen in Eq. (20) must have $\mathrm{Re}q(\omega)>0$ for stable waves with $G<1$; otherwise the Green's function diverges with increasing r, which is unphysical. For $G\approx0$ and $\omega=0$,

$$G(r,0)=\frac{\gamma_e^2G}{2\pi a_{ee}v^2}K_0(\gamma_er/v). \tag{21}$$

Apart from the factor $G/a_{ee}=g\rho_e$, which represents the net gain in generating Q_s from Q_e, this is simply the static Green's function derived previously [1].

The coordinate-space Green's function can be written in terms of Eq. (12) as

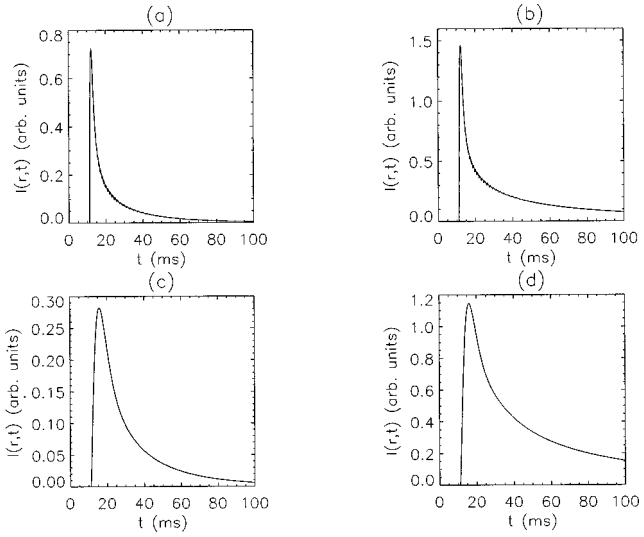

FIG. 1. Integrals $I(r,t)=2\pi a_{ee}v^2G(r,t)/\gamma_e^2G$ from the Green's function formula (22) vs t for $r=0.1$ m, $v=9$ m s^{-1}, $\gamma_e=108$ s^{-1}, $a_{ee}=0.853$, $Q_e^{(0)}=0.0103$, and $C=1.82$ with (a) $G=0.57$, $\alpha=\beta=2000$ s^{-1}; (b) $G=0.95$, $\alpha=\beta=2000$ s^{-1}; (c) $G=0.57$, $\alpha=\beta=400$ s^{-1}; and (d) $G=0.95$, $\alpha=\beta=400$ s^{-1}.

$$G(r,t)=\frac{\gamma_e^2G}{2\pi a_{ee}v^2}\int\frac{d\omega}{2\pi}e^{-i\omega t}L(\omega)K_0[q(\omega)r]. \quad (22)$$

Unfortunately, the integral in Eq. (22) does not appear to be expressible in terms of tabulated functions, except in certain limiting cases. One important such case is the limit in which $\alpha,\beta\gg\omega$ and $G\approx0$, where $L(\omega)\approx1$ and

$$G(r,t)=\frac{\gamma_e^2Ge^{-\gamma_e t}}{2\pi a_{ee}v}\frac{1}{\sqrt{v^2t^2-r^2}}\Theta(vt-r), \quad (23)$$

where Θ denotes a unit step function. This result is the Green's function for $D_e(\mathbf{k},\omega)=0$, i.e., for the standard two-dimensional, damped wave equation.

Figure 1 shows the integral in Eq. (22), which we denote as $I(r,t)$, for fixed r as a function of time for a variety of parameters. For large α and β (short dendritic integration times) and small to moderate gain G, Fig. 1(a) shows that the Green's function is sharply peaked just after the minimum propagation time $r/v\approx11$ ms to the point in question. This compares with the algebraic singularity of Eq. (23) in the limit $\alpha,\beta\to\infty$. For larger G, Fig. 1(b) shows that the Green's function is increased in magnitude [even more so when $G(r,t)$ rather than the integral $I(r,t)$ is considered] and broadened in time, owing to a greater degree of ''regeneration'' of neural pulses at sites away from the origin when the gain is large. Corresponding results for smaller α and β are shown in Figs. 1(c) and 1(d). Here the longer dendritic integration time leads to additional broadening of the response as a function of time and a consequent reduction in the peak magnitude of $I(r,t)$ relative to Figs. 1(a) and 1(c).

D. Correlation functions and spectra

The excitatory wave potential $\phi_e(r,\omega)$ at r due to a monochromatic point source is given by the product of Eq. (19) with $Q_s(\omega)$. The unnormalized second-order correlation function between a potential ϕ_{em} due to a more general source at $\mathbf{R}_m$ and ϕ_{en} due to a source at $\mathbf{R}_n$ is given by

$$C_{mn}(\mathbf{r},\mathbf{r}',\tau)=\langle[\phi_{em}(\mathbf{r},t)-\langle\phi_{em}(\mathbf{r},t)\rangle]\times[\phi_{en}^*(\mathbf{r}',t+\tau)-\langle\phi_{en}^*(\mathbf{r}',t+\tau)\rangle]\rangle \quad (24)$$

$$=\int\frac{d\omega}{2\pi}e^{-i\omega\tau}\phi_{em}(\mathbf{r},\omega)\phi_{en}^*(\mathbf{r}',\omega), \quad (25)$$

$$=\left(\frac{\gamma_e^2G}{2\pi a_{ee}v^2}\right)^2\int\frac{d\omega}{2\pi}e^{-i\omega\tau}|L(\omega)|^2\times Q_{sm}(\omega)Q_{sn}^*(\omega)K_0[q(\omega)r_m]K_0^*[q(\omega)r_n'], \quad (26)$$

where angle brackets denote an average over t (over a time long compared to the phenomena of interest, which principally occur on time scales much less than 1 s), $r_m=|\mathbf{r}-\mathbf{R}_m|$, $r_n'=|\mathbf{r}'-\mathbf{R}_n|$, and we have set $M_e=1$ in Eq. (8) without loss of generality. Note that $Q_{sm}(0)=0$ for all m in accordance with the definition in Sec. II A, we have used the fact that $\phi_e(\mathbf{r},t)$ is real for all $\mathbf{r}$ and there is assumed to be no correlation between different frequency components of any one source beyond the correlation implied by the reality of $\phi_e(\mathbf{r},t)$. Also, $|K_0|$ and $|L|$ both decrease at large ω for $G<1$ in Eq. (26).

In the limit with $\alpha,\beta\gg\omega$ and small G, one can approximate the integral in Eq. (26) for white-noise sources. Denoting this integral by I_{mn}, we find [21]

$$I_{mn}\approx\frac{\pi v}{2\sqrt{r_mr_n'}}\exp[-\gamma_e(r_m+r_n')/v]\int\frac{d\omega}{2\pi}\frac{1}{(\gamma_e^2+\omega^2)^{1/2}}\times\exp[-i\omega\tau+i\omega(r_m-r_n')/v] \quad (27)$$

$$=\frac{v}{2\sqrt{r_mr_n'}}\exp[-\gamma_e(r_m+r_n')/v]\times K_0[\gamma_e|\tau+(r_n'-r_m)/v|]. \quad (28)$$

The result (28) is included for completeness, but is not used in what follows.

The total correlation function due to several sources is

$$C(\mathbf{r},\mathbf{r}',\tau)=\sum_{m,n}C_{mn}(\mathbf{r},\mathbf{r}',\tau). \quad (29)$$

The normalized correlation function can be written as

$$\tilde{C}(\mathbf{r},\mathbf{r}',\tau)=\frac{C(\mathbf{r},\mathbf{r}',\tau)}{[C(\mathbf{r},\mathbf{r},0)C(\mathbf{r}',\mathbf{r}',0)]^{1/2}}, \quad (30)$$

which is unity if $\mathbf{r}=\mathbf{r}'$ and $\tau=0$. The variance of ϕ_e at $\mathbf{r}$ is

$$\langle|\phi_e-\langle\phi_e(\mathbf{r})\rangle|^2\rangle=\mathrm{var}[\phi_e(\mathbf{r})]=C(\mathbf{r},\mathbf{r},0). \quad (31)$$

For points near a particular source the correlation function and the variance are dominated by that source, owing to the singularity in $K_0(z)$ at small z [22].

Useful limiting forms of the normalized correlation coefficient for two sources can be obtained when one source dominates at $\mathbf{r}'$ or when both sources have the same amplitude there. Denoting the fluctuating part of ϕ_{en} by f_n at $\mathbf{r}$ and f_n' at $\mathbf{r}'$ and noting that these quantities are real, we can write

$$\widetilde{C}(\mathbf{r},\mathbf{r}',\tau)=\frac{\langle(f_1+f_2)(f_1'+f_2')\rangle}{[\langle(f_1+f_2)^2\rangle\langle(f_1'+f_2')^2\rangle]^{1/2}}. \tag{32}$$

If one source (say 1) dominates over the other at $\mathbf{r}'$ and signals from the two sources have equal amplitudes at $\mathbf{r}$, Eq. (32) then implies $\widetilde{C}\approx\widetilde{C}_{11}/\sqrt{2}$ if the sources are uncorrelated and $\widetilde{C}\approx\widetilde{C}_{11}$ if they are completely correlated. (Here we use the notation $\widetilde{C}_{11}$ to denote the normalized correlation due to source 1 alone.) This case applies when $\mathbf{r}'$ is significantly closer to one source than the other. If the amplitudes of the signals from the two sources are equal at both points being correlated one always finds $\widetilde{C}=\widetilde{C}_{11}$.

The power spectrum $P(\mathbf{r},\omega)$ is the Fourier transform of $C(\mathbf{r},\mathbf{r},t)$:

$$P(\mathbf{r},\omega)=\sum_{m,n}\phi_{em}(\mathbf{r},\omega)\phi_{en}^*(\mathbf{r},\omega), \tag{33}$$

$$=\left(\frac{\gamma_e^2 G}{2\pi a_{ee}v^2}\right)^2\sum_{m,n}|L(\omega)|^2 Q_{sm}(\omega)Q_{sn}^*(\omega)$$

$$\times K_0[q(\omega)r_m]K_0^*[q(\omega)r_n]. \tag{34}$$

For the case of a point midway between two sources with identical power spectra

$$P(\mathbf{r},\omega)=A\left(\frac{\gamma_e^2 G}{2\pi a_{ee}v^2}\right)^2|L(\omega)Q_s(\omega)K_0[q(\omega)a]|^2, \tag{35}$$

where $2a$ is the separation of the sources, $A=4$ if the sources are perfectly correlated, $A=2$ if they are uncorrelated, and $A=1$ for a single source. At points significantly closer to one source than the other, the spectrum is dominated by that of the closer source.

If we denote the argument of any Macdonald function in the previous expressions by z, the relationship $|\arg z|<\pi/2$ must hold for stable waves since otherwise the relevant expressions would diverge unphysically at large r [22]. In this regime $K_0(z)$ can be rapidly evaluated numerically from the integral form

$$K_0(z)=\int_0^\infty e^{-z\cosh t}dt. \tag{36}$$

Provided its argument is not too small, the function K_0 can be approximated as

$$K_0(z)\approx\sqrt{\frac{\pi}{2z}}e^{-z}, \tag{37}$$

which is very fast to evaluate and permits further analytic treatment in some limiting cases. For real z at least, this approximation is semiquantitatively correct provided $\mathrm{Re}z\gtrsim 0.1$ and improves in accuracy for large $|z|$, with a fractional error of approximately $-1/8z$ [22].

Equations (34), (35), and (37) enable the asymptotic form of the power spectrum to be determined. For example, midway between two white noise sources one has

$$P(\mathbf{r},\omega)\sim\begin{cases}\omega^{-5}, & \omega\gg\alpha,\beta,\gamma_e & (38)\\ \omega^{-4}, & \gamma_e\gg\omega\gg\alpha,\beta & (39)\\ \omega^{-3}, & \beta\gg\omega\gg\alpha,\gamma_e & (40)\\ \omega^{-2}, & \beta,\gamma_e\gg\omega\gg\alpha & (41)\\ \omega^{-1}, & \alpha,\beta\gg\omega\gg\gamma_e & (42)\\ \text{const}, & \alpha,\beta,\gamma_e\gg\omega. & (43)\end{cases}$$

Note that $\beta>\alpha$ has been assumed without loss of generality. It is also worth noting that the strong inequalities in Eqs. (39)–(42) are seldom well satisfied in humans since α, β, and γ_e are typically of the same order [1].

Before proceeding, we stress that all the above analysis is for an infinite cortex. If a finite cortex is to be studied more accurately, we should replace Eq. (16) by a sum over all allowed wave vectors. This sum will then appear in subsequent formulas. However, if nonuniform ($k\neq 0$) modes are strongly damped (as our previous work has implied [1]), boundary conditions will not have a strong role because (i) the modes will be indistinguishable due to frequency broadening and (ii) the modes will not be much affected by boundaries if they largely dissipate before reaching them.

III. NUMERICAL RESULTS

In this section we evaluate a range of properties of cortical oscillations driven by white-noise sources, including the correlation function, variance, and power spectrum. By exploring the effects of varying the cortical parameters and the degree of phase coherence between the sources, these results enable us to exhibit a robust candidate mechanism for what has been termed synchronous oscillation. A full parameter survey is not carried out since it is not needed for our main aim of establishing the existence of the key phenomena.

In this study we use a ''canonical'' set of parameters unless otherwise stated. These values are chosen for the purposes of illustration and to provide continuity with previous work. Except for α and β, the canonical values used are the same as in our previous work [1], namely, $v=9$ m s^{-1}, $\gamma_e=108$ s^{-1}, $g=36$, $a_{ee}=0.853$, $Q_e^{(0)}=0.0103$, $C=1.82$, $G=0.57$, and $\alpha=\beta=400$ s^{-1}. We have adopted larger values of α and β here than previously to model more accurately dendritic integration with a mean response time of 5 ms (previously we had $\alpha=100$ s^{-1} and $\beta=350$ s^{-1}, giving a *peak* response at 5 ms). The full Macdonald functions are used in evaluating analytic expressions from Sec. II, al-

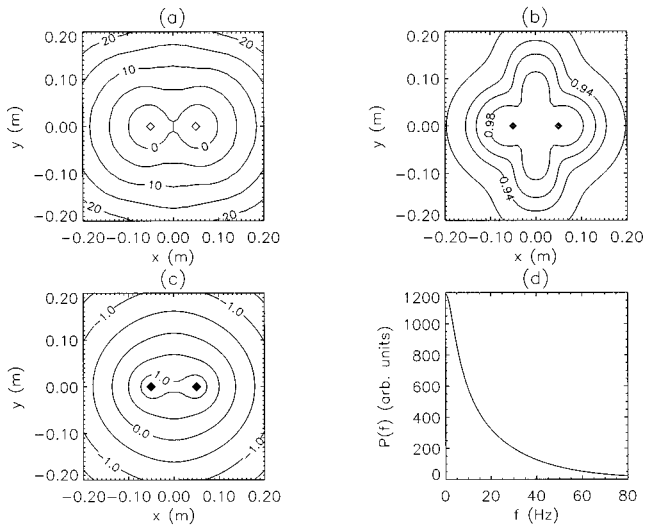

FIG. 2. Wave quantities for two correlated sources and the canonical parameters listed at the start of Sec. III. (a) Time of maximum correlation $t_{\max}$ (ms) vs position. (b) Maximum correlation $\tilde{C}_{\max}$ vs position. Note that in this and subsequent figures contours of this quantity are drawn at levels 0.98, 0.96, 0.94, 0.92, 0.9, 0.8, 0.7, and 0.6, as required. (c) Variance $\log_{10}C(\mathbf{r},\mathbf{r},0)$ vs position. (d) Power spectrum at the origin vs frequency.

though we have found that the approximation (37) is a good one for most purposes.

A. Correlated sources

Figure 2 shows results for driving by a pair of perfectly correlated white-noise sources of unit amplitude with the canonical parameters. The sources are correlated with each other, but different frequency components of a given source are mutually uncorrelated here and in all succeeding figures. Each source was constructed for the purposes of numerically evaluating the analytical expressions by choosing components of fixed amplitude but random relative phase, distributed equally in frequency from zero to a maximum frequency ($\sim 10^4$ s^{-1}) far higher than any inverse time scales relevant to the problem. In the present case, the phases of the two sources were chosen to be identical at each frequency to produce perfect correlation, but the relative phases of different frequency components were random.

In Fig. 2(a) we plot the time $t_{\max}$ of maximum positive correlation $\tilde{C}(\mathbf{0},\mathbf{r}',t)$ as a function of position $\mathbf{r}'$, with the origin at the center of the frame and the sources on the x axis a distance $2a=0.1$ m apart. The correlation function was determined by Fourier transforming the power spectrum and then $t_{\max}$ was found by searching directly for the global maximum. The uncertainty in $t_{\max}$ was less than 0.25 ms. The value of $t_{\max}$ increases toward the outside of the figure, reflecting the outward propagation of waves from the two sources (near which $t_{\max}$ is negative, with the innermost contour drawn at -10 ms). At large distances the contours approach circles, as expected for outward propagating waves from a single source (the sources cannot be distinguished at large ranges). Near each source $t_{\max}$ is negative because a given wave crest arrives there before it reaches the reference point at the origin, while the locus of zero-lag correlation is a figure-eight passing through the origin and determined by the interplay between the relative path lengths to the points in question and the relative amplitudes of the two signals.

One important point is that the correlation has the spatial dependence of self-correlations C_{mm} alone. This can be seen by substituting $r_1=r_2=a$ into Eq. (26) for correlations relative to the origin, which gives

$$C(0,\mathbf{r}',\tau)=\left(\frac{\gamma_e^2 G}{2\pi a_{ee}v^2}\right)^2\int\frac{d\omega}{2\pi}e^{-i\omega\tau}|L(\omega)|^2 \times K_0[q(\omega)a][Q_{s1}(\omega)+Q_{s2}(\omega)] \times\{Q_{s1}(\omega)K_0[q(\omega)r_1']+Q_{s2}(\omega)K_0[q(\omega)r_2']\}^*. \tag{44}$$

We see from this expression that all the terms are of the same form as those in C_{11} and C_{22} and that both of these terms are important. The only role played by the relative correlation between the sources is to determine the number of factors of $|Q_{s1}|^2$ that will appear in the final expression. This result is in accord with the discussion following Eq. (35).

Figure 2(b) shows $\tilde{C}_{\max}$, the maximum positive correlation $\tilde{C}(\mathbf{0},\mathbf{r}',t)$, as a function of $\mathbf{r}'$. A broad maximum of near-perfect correlation is seen near the center of the figure, decreasing slowly toward the edges. Naively, one might expect perfect correlation at all points for perfectly correlated sources. However, two-dimensional (2D) wave equations do not yield δ-function propagators (see Fig. 1, for example) and this reduces the correlation below unity at large ranges. We explore this point further in Sec. III B. The remaining point visible in Fig. 2(b) is the pair of features at the sources. The lowered correlation here is due to the dominance of a single source, as explained following Eq. (32).

Figure 2(c) shows the variance $C(\mathbf{r},\mathbf{r},0)$ as a function of $\mathbf{r}$. This quantity is seen to fall off approximately exponentially with distance from each source at large distances (as seen by the nearly uniformly spaced logarithmic contours). This reflects the exponential distribution of axonal ranges. The two strong peaks are at the sources, where the response is singular.

The power spectrum (35), evaluated at the midpoint between the sources, is seen in Fig. 2(d). It exhibits a strong peak at low frequencies, falling to half maximum near 9.5 Hz. (Note that the zero-frequency component is zero in conformity with our definition.) At very low frequencies we find that the scaling (43) is approached, while the result (38) is approached at high frequencies. However, because of the relative proximity of the values of α,β, and γ_e, the exponents in Eqs. (39)–(42) are not clearly manifest.

Figure 3 shows results from a numerical simulation of the full nonlinear partial differential equations (1)–(7) carried out for the canonical parameters using the same methods as in our previous work [1], but omitting inhibitory effects in accord with the approximations made here. The driven points were at $x=\pm a$, which for the 81×81 grid used here corresponds to ± 7 grid units with respect to the center. The driving signal at these points [Q_s in Eqs. (6) and (7)] was the same zero-mean Gaussian white noise, with a standard de-

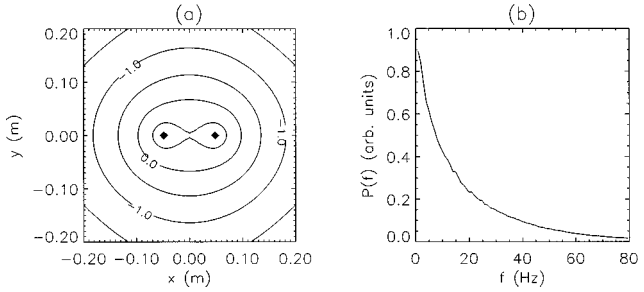

FIG. 3. Wave quantities from numerical simulations of the full nonlinear equations (1)–(7) for the same parameters as in Fig. 2, but expressed in different arbitrary units. (a) Variance $\log_{10}C(\mathbf{r},\mathbf{r},0)$ vs position. (b) Power spectrum at the origin vs frequency.

viation in the time domain of 0.010 (much smaller than the steady-state driving), which was small enough to avoid nonlinear effects. Figure 3 is the result of a simulation lasting 132 s with a step size of 0.25 ms. Figure 3(a) shows that the variance (computed directly by accumulating mean and mean-square field values at each grid point) has a very similar form to that in Fig. 2(c), while Fig. 3(b) shows that the corresponding power spectrum (computed by compiling and then Fourier transforming a time series over the entire simulation) at $\mathbf{r}=\mathbf{0}$ is also very similar to that in Fig. 2(d), with the half-power point occurring between 9 and 9.5 Hz, close to the value of 9.5 Hz in the canonical case. A fully linearized simulation also has been carried out with equivalent results, consistent with nonlinear effects not being important to the results shown in Fig. 3. The similarity between Figs. 2(c) and 2(d), on the one hand, and Figs. 3(a) and 3(b), on the other, demonstrates that boundary conditions are not important in determining the correlation and spectral properties of the wave fields in this case: Fig. 2 is for an infinite medium, while Fig. 3 was calculated using periodic boundary conditions. This insensitivity to boundary conditions arises because the waves are relatively strongly damped. Robinson *et al.* [1] showed that the width of modal resonances exceeded their separation for typical cortical parameters, obliterating the modal structure of spectra; this result evidently carries over to the correlation properties considered here.

B. Single source

Figure 4 shows a situation with the canonical parameters, except that the amplitude of the second source (at $x=+a$) has been reduced to zero. The $t_{\max}$ plot in Fig. 4(a) is consistent with the two-source plot seen in Fig. 2(a) being the superposition of two single-source plots with the same phase, i.e., with self-correlations C_{mm} dominating in Eq. (29). The velocity of propagation of the point of maximum positive correlation, obtained from the ratio of the distance traveled to $t_{\max}$, is approximately 8.5 m s^{-1}. This is not the same as the velocity v of the waves because of the broadening of the Green's function seen in Fig. 1, which weights times greater than r/v more strongly than in the limit $\alpha,\beta\to\infty$, $G\to 0$.

Close analysis of the results in Fig. 4(b) shows that $\tilde{C}_{\max}$ actually has a minimum at the source (the innermost contours shown correspond to values below 0.98, the value at the innermost labeled contour). This results from the imperfect correlation between points at different distances from the

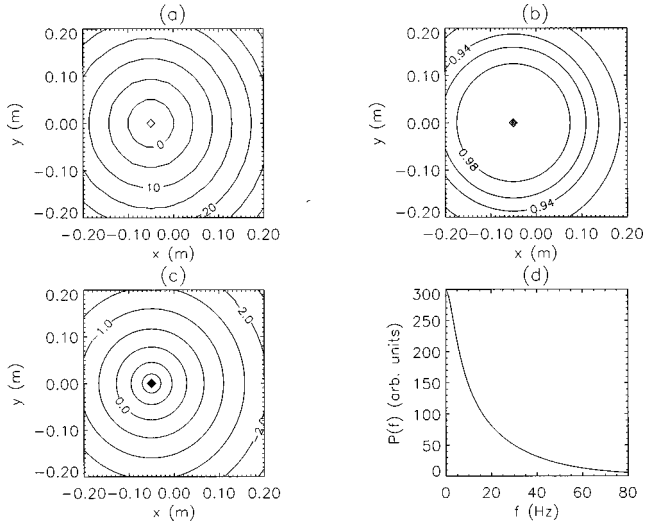

FIG. 4. Wave quantities for a single source and the canonical parameters listed at the start of Sec. III. (a) Time of maximum correlation $t_{\max}$ (ms) vs position. (b) Maximum correlation $\tilde{C}_{\max}$ vs position. (c) Variance $\log_{10}C(\mathbf{r},\mathbf{r},0)$ vs position. (d) Power spectrum at the origin vs frequency.

source owing to the non-δ-function form of the 2D propagator. The maximum occurs on the circle $r_1=r_1'=a$. The variance plot in Fig. 4(c) is accordingly modified and the power spectrum in Fig. 4(d) is reduced by the expected factor of four relative to that in Fig. 2(d) [cf. Eq. (35)].

C. Uncorrelated sources

Figure 5 shows results for a pair of equal-amplitude *uncorrelated* (i.e., whose relative phase at a given frequency is a random number chosen between 0 and 2π, in addition to all frequency components having random relative phase, as before) sources having the canonical parameters. In accordance with the remarks in the preceding section, the plot

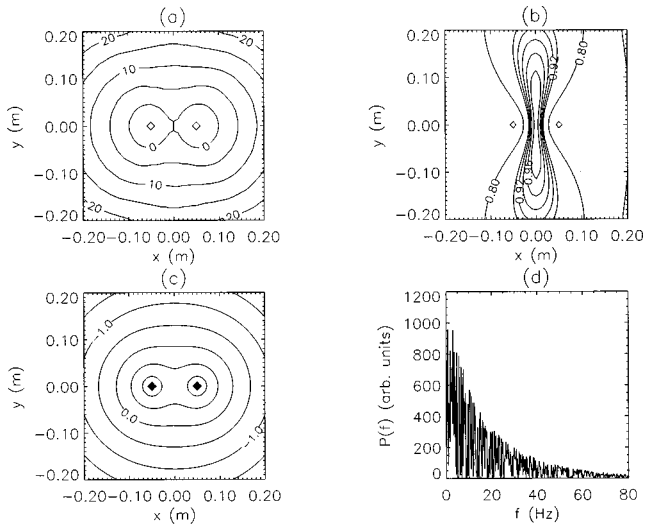

FIG. 5. Wave quantities for two uncorrelated sources and the canonical parameters listed at the start of Sec. III. (a) Time of maximum correlation $t_{\max}$ (ms) vs position. (b) Maximum correlation $\tilde{C}_{\max}$ vs position. (c) Variance $\log_{10}C(\mathbf{r},\mathbf{r},0)$ vs position. (d) Power spectrum at the origin vs frequency.

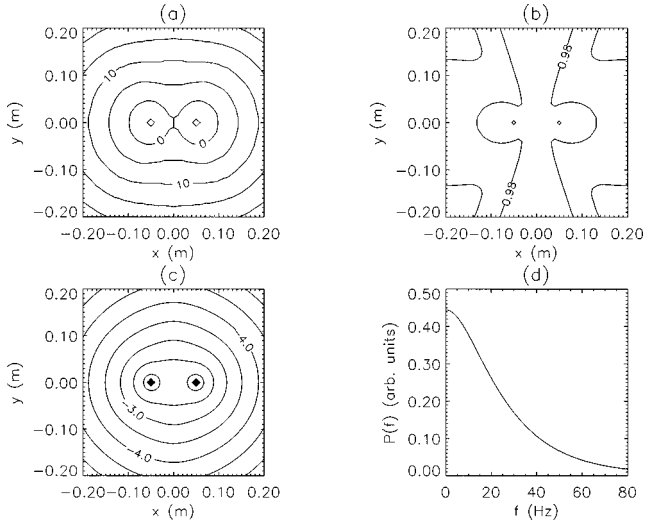

FIG. 6. Wave quantities for two correlated sources and the canonical parameters listed at the start of Sec. III, except that the gain $G=0.015$. (a) Time of maximum correlation $t_{\max}$ (ms) vs position. (b) Maximum correlation $\tilde{C}_{\max}$ vs position. (c) Variance $\log_{10}C(\mathbf{r},\mathbf{r},0)$ vs position. (d) Power spectrum at the origin vs frequency.

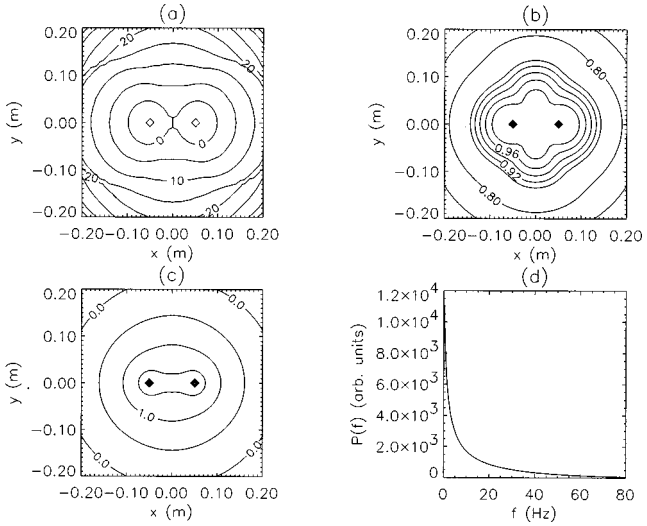

FIG. 7. Wave quantities for two correlated sources and the canonical parameters listed at the start of Sec. III, except that the gain $G=0.95$. (a) Time of maximum correlation $t_{\max}$ (ms) vs position. (b) Maximum correlation $\tilde{C}_{\max}$ vs position. (c) Variance $\log_{10}C(\mathbf{r},\mathbf{r},0)$ vs position. (d) Power spectrum at the origin vs frequency.

of $t_{\max}$ in Fig. 5(a) is almost identical to Fig. 2(a) in this case, consistent with our picture of outwardly propagating waves whose time of maximum correlation with the origin is determined by self-correlations rather than the degree of cross correlation between the sources.

The plot of $\tilde{C}_{\max}$ in Fig. 5(b) is very different from the corresponding plot in Fig. 2(b). Near-perfect correlation is seen near the origin, falling off slowly along the y axis at a similar rate to that in Fig. 2(b), but much more rapidly in the x direction. Both features are consistent with the discussion following Eq. (32). (i) On the y axis, the amplitudes of the two signals are equal and $\tilde{C}=\tilde{C}_{11}$. (ii) Near either source, that source's signal will dominate over the signal from the other source. Hence we expect $\tilde{C}\approx\tilde{C}_{11}/\sqrt{2}\approx 1/\sqrt{2}$, consistent with the numerical value of just under 0.7. (iii) Far from both sources in the x direction, the nearer source will again dominate and we expect the correlation function to decline toward $\tilde{C}_{11}/\sqrt{2}$, which is again consistent with Fig. 5(b).

The variance plot in Fig. 5(c) is very similar to that in Fig. 2(c), except that the variance at large distances from the sources is smaller owing to their lack of correlation. In Fig. 5(d) we see that the power spectrum fluctuates between zero and the value for perfectly correlated sources, with an average of half that value. (The fluctuations occur because the relative phase between the sources at a given frequency has a single, randomly chosen value; phase is not averaged over at each frequency, although this could be done.) When smoothed with respect to frequency (or, equivalently, when averaged over many realizations of the phase distribution), the results in Fig. 5(d) correspond to the predicted value $A=2$ in Eq. (35).

D. Effect of cortical gain

Reduction of G from 0.57 in the canonical case to 0.015 ($g=1$) scarcely changes the plot of $t_{\max}$ in Fig. 6(a) from the corresponding one in Fig. 2(a), consistent with dominance of self-correlations. In Fig. 6(b) the region of near-perfect correlation is extended relative to Fig. 2(b), a consequence of reduction in magnitude of the tail of the Green's function with decreasing G that was seen in Figs. 1(c) and 1(d). Consistent with this interpretation, the velocity of the point of maximum correlation is found to be almost indistinguishable from $v=9\ \mathrm{m\,s^{-1}}$ in Fig. 2(b). Figure 6(c) shows that the variance is reduced relative to that in Fig. 2(c), principally owing to the first G-dependent factor in Eq. (26). However, the shapes of the contours are very similar. Likewise, the spectral power is reduced by approximately the same factor in Fig. 6(d). Here we also see that the half-power frequency is about 23 Hz, compared to 9.5 Hz in the canonical case. Robinson *et al.* [1] showed that there low-frequency wave modes become less damped as G increases, with the least damping at $f=0$. Hence one can expect a narrower spectral profile for small G.

In Fig. 7(a) we find that the central regions of the $t_{\max}$ plot are only slightly changed from Fig. 2(a), although $g=60$ and $G=0.95$ in this case. In the outer regions, however, the contours of $t_{\max}$ undergo a sharper changeover from near-field to far-field behavior. Consistent with the temporal broadening of the Green's function for large G, seen in Fig. 1(d), Fig. 7(b) shows that the correlation function decreases more steeply at large distances than in Fig. 2(b). The variance plot in Fig. 7(c) is similar to that in Fig. 2(c), although the values are higher because of the larger value of G. The nearness to an instability at $f=0$ (which sets in at $G=1$ [1]) causes the power spectrum to be very strongly peaked at low frequencies, with Fig. 7(d) showing the half-power point at only 2 Hz.

E. Variation of relative phase of correlated sources

A series of runs has been done in which the phase of source 2 (at $x=+a$) has been advanced relative to source 1

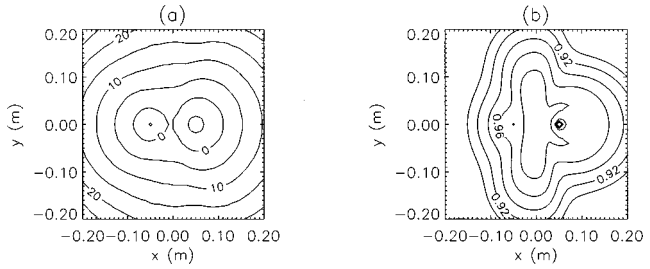

FIG. 8. Wave quantities for two correlated sources and the canonical parameters listed at the start of Sec. III, except that the right source leads the left one by $\pi/4$. (a) Time of maximum correlation $t_{\max}$ (ms) vs position. (b) Maximum correlation $\tilde{C}_{\max}$ vs position.

(at $x=-a$), while maintaining their correlation. Figures 8 and 9 show results for phase advances of $\pi/4$ and $\pi/2$, respectively.

As the phase difference increases, Figs. 8(a) and 9(a) show that the zone of negative $t_{\max}$ around source 2 increases, while that around source 1 decreases and eventually disappears for a phase difference of roughly $\pi/2$. Likewise, Figs. 8(b) and 9(b) show that the correlation plots become increasingly asymmetric owing to the changed relative lag introduced by the phase shift of source 2. All of these trends are consistent with our picture of the dominance of the two single-source self-correlations in determining the synchrony properties of the cortex.

F. Effect of dendritic integration

Figure 10 shows results for a case in which we have set $\alpha=\beta=2\times10^3\ \mathrm{s}^{-1}$ to minimize the effects of the dendritic integration time. (We do not argue that a value this large would be appropriate for a real cortex.) The results in Figs. 10(a) and 10(c) are very similar to those seen in the canonical case. The correlation plot in Fig. 10(b) shows a narrower zone of very high correlation relative to Fig. 2(b), owing to the narrower form of the Green's function for high α and β [see Fig. 1(a)], which requires a closer match between path lengths from the two sources for high correlations to exist. One should note that the sources are surrounded by regions of lowered correlation [cf. the discussion after Eq. (32)]. The power spectrum in Fig. 10(d) has a much longer high-frequency tail than the canonical one, with the half-power

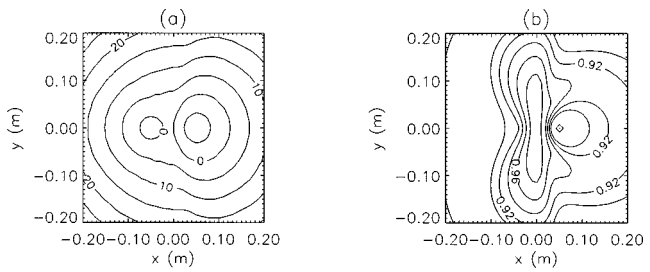

FIG. 9. Wave quantities for two correlated sources and the canonical parameters listed at the start of Sec. III, except that the right source leads the left one by $\pi/2$. (a) Time of maximum correlation $t_{\max}$ vs position. (b) Maximum correlation $\tilde{C}_{\max}$ vs position.

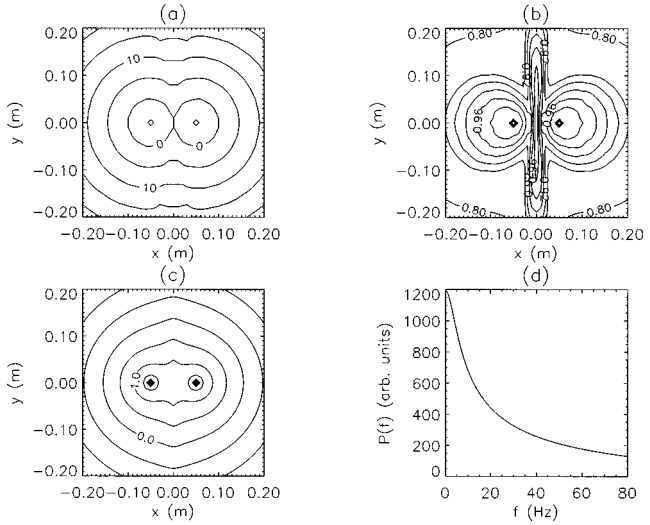

FIG. 10. Wave quantities for two correlated sources and the canonical parameters listed at the start of Sec. III, except that $\alpha=\beta=2000\ \mathrm{s}^{-1}$. (a) Time of maximum correlation $t_{\max}$ (ms) vs position. (b) Maximum correlation $\tilde{C}_{\max}$ vs position. (c) Variance $\log_{10}C(\mathbf{r},\mathbf{r},0)$ vs position. (d) Power spectrum at the origin vs frequency.

point at 12 Hz. This is consistent with Eq. (42) due to the relative unimportance of dendritic low-pass filtering in this case.

IV. DISCUSSION AND CONCLUSIONS

We have studied the dynamics of a cortex driven by a finite number of white-noise sources using our wave-equation formalism. We have computed Green's functions, power spectra, fluctuation levels, and correlation functions analytically and numerically. The results obtained here reproduce the main features of zero-lag correlations (synchronous oscillation) observed physiologically and defined to be cross correlations that are maximal at zero time lag. They confirm numerical results reported by Wright [20] and extend these earlier results by showing that zero-lag cross correlation between two excited sites on the simulated cortical surface can be described by an expression in which only propagation time lags and wave amplitudes in the linked excitatory elements are of relevance. They show that the most important contributions are from self-correlations of each source with itself (in general *both* sources' self-correlations are significant at a given point), regardless of the degree of mutual correlation between sources. This result thus carries over immediately to multiple sources. Zero-lag cross correlation of this sort is therefore expected to be a widely occurring property of neural nets, including real cortical neurons.

It should be stressed that the zero-lag cross-correlation results that we have found do not result from the existence of very weakly damped or growing global eigenmodes of the cortex: Indeed, there are no such modes under the circumstances discussed. Nor does it depend strongly on local inhibition in the regimes investigated. Qualifications to these conclusions are discussed in points (i)–(iii) below.

Since the determination of neuronal couplings to high accuracy is very difficult in most experimental situations, it

should be noted that our model makes predictions about the generation of nonzero-lag wave motions in the neural field around the locus of zero-lag synchrony. The occurrence of traveling waves surrounding the fields of synchrony should be fairly readily demonstrable, but has not been looked for in any experiment to date, to the best of the authors' knowledge. Such surrounding wave motion might be more readily observed in local-field potentials or electrocorticogram rather than in pulse activity, given the problems of adequate sampling in ongoing pulse trains.

The present model is not in contradiction with alternate mechanisms of synchrony and synchronous oscillation, such as nonlinear phase locking or cortical driving by synchronous inputs [9–11,13]. Both these processes may supplement the present mechanism. While zero-lag synchrony can emerge in the absence of any synchrony in the inputs, this is not a necessary condition. The essentially linear mechanism described here might also act to entrain local nonlinear phase locking among individual neurons. Likewise, there is no necessary contradiction with observations of intrinsic rhythmicity of firing in single cells, often associated with synchronous oscillation [9,10,23]. Certain models of learning depending on changes in synaptic strength indicate that cells with intrinsic rhythmicity would emerge as a consequence of induced rhythmic and synchronous firing within a population of real neurons [24].

Qualifications to our work are that real neurons have complicated properties in addition to those represented approximately in our model and that experimental observations of real neural synchrony are made in circumstances much more elaborate than can be represented by the introduction of noise inputs to two points on a plane. Nonetheless, this model appears to provide a mechanism for the occurrence of zero-lag maximum cross correlations in physiological observations, predicts a range of other observable quantities (e.g., variance and power spectra), and might be extended to cover a wider range of the relevant phenomena when appropriate allowance is made for complicating factors such as the following points.

(i) To a first approximation, our results appear adequate to explain the principal qualitative physiological finding upon which most subsequent work has been based, i.e., excitation of two points on the cortical surface by distinct, unrelated inputs causes activity on a locus in the vicinity of the inputs to attain zero-lag cross correlation [5]. The present match to experiment is qualitative only and no regard has been given to the inhomogeneity of real interneuronal coupling. The precise details of intercellular couplings, delay, and synaptic gain factors (which are not routinely measured) need to be determined in physiological experiments before our model can be fully quantitatively tested. A further physiologically important factor we have omitted is that of nonlinear dynamic influences on gain. Such effects can be nonuniform and will occur where stimuli are large enough to yield significant nonlinear responses (linear terms are included here). In physiological terms, nonuniform gain may arise from the action of the reticular activating system [6,20].

(ii) Although our results show that local inhibition is a small effect, it should be noted that the inhibitory connectivities are not precisely known. Also, the effectiveness of inhibition may be modulated via dynamical feedback via chemical neurotransmitters and neuromodulators acting on time scales ranging from milliseconds to seconds and longer. These effects, which are likely to depend strongly on brain state (e.g., attentive, relaxed, and sleeping), must be included in a full model of electrocortical wave activity and we are currently in the process of generalizing our model to incorporate them. It is possible that these effects could allow the cortex to cross the linear stability threshold ($G=1$) into regimes of nonlinear dynamics, including limit-cycle oscillations or chaos, for example, without necessarily entering a state of near-maximum Q_e. Weakly damped or growing waves (and hence the precise boundary conditions) would likely play a more important role in such regimes than for the parameters considered here.

(iii) No account is given in the present model for the frequent occurrence of gamma-band oscillation in association with pulse synchrony. This association has been partially accounted for by Wright [20] and will be considered further in future work.

ACKNOWLEDGMENTS

P.A.R. and C.J.R. thank the University of Iowa and the Mental Health Research Institute of Victoria for their hospitality during visits on which some of this work was undertaken. This work was supported by the Australian Academy of Science and the Ross Trust, Melbourne.

[1] P. A. Robinson, C. J. Rennie, and J. J. Wright, Phys. Rev. E **56**, 826 (1997).
[2] R. Eckhorn, B. Bauer, W. Jordon, M. Brosch, W. Kruse, M. Munk, and H. J. Reitboeck, Biol. Cybern. **60**, 121 (1988).
[3] C. M. Gray, P. König, A. K. Engel, and W. Singer, Nature (London) **338**, 334 (1989).
[4] W. Singer, in *Large-Scale Neuronal Theories of the Brain*, edited by C. Koch and J. Davis (MIT, Cambridge, MA, 1994).
[5] W. Singer and C. M. Gray, Annu. Rev. Neurosci. **18**, 555 (1995).
[6] M. H. J. Munk, P. R. Roelfsma, P. König, A. K. Engel, and W. Singer, Science **272**, 271 (1996).
[7] P. König, A. K. Engel, and W. Singer, Proc. Natl. Acad. Sci. USA **92**, 290 (1995).
[8] B. Schechter, Science **274**, 339 (1996).
[9] R. R. Llinas, A. A. Grace, and Y. Yarom, Proc. Natl. Acad. Sci. USA **88**, 897 (1991).
[10] M. Steriade, R. Curro-Dossi, and D. Contreras, Neuroscience (Oxford) **56**, 1 (1993).
[11] P. Tass and H. Haken, Biol. Cybern. **74**, 31 (1996).
[12] Y. Kuramoto and I. Nishikawa, J. Stat. Phys. **49**, 569 (1987).
[13] H. Nischwitz and A. Glunder, Biol. Cybern. **73**, 389 (1995).
[14] H. R. Arnoldi and W. Brauer, Biol. Cybern. **74**, 209 (1996).
[15] R. D. Traub, M. A. Whittington, I. M. Stanford, and J. G. R.

Jeffereys, Nature (London) **383**, 621 (1996).
[16] W. J. Freeman, *Mass Action in the Nervous System* (Academic, New York, 1975).
[17] P. L. Nunez, in *Neocortical Dynamics and Human EEG Rhythms*, edited by P. L. Nunez (Oxford University Press, Oxford, 1995).
[18] J. J. Wright and D. T. J. Liley, Biol. Cybern. **72**, 347 (1995).
[19] J. J. Wright and D. T. J. Liley, Behav. Brain Sci. **19**, 285 (1996).
[20] J. J. Wright, Biol. Cybern. **76**, 181 (1997).
[21] I. S. Gradshteyn and I. M. Ryzhik, *Table of Integrals, Series and Products* (Academic, San Diego, 1994).
[22] *Handbook of Mathematical Functions*, edited by M. Abramowitz and I. A. Stegun (Dover, New York, 1970).
[23] C. M. Gray and D. A. McCormick, Science **274**, 109 (1996).
[24] G. Parisi, J. Phys. A **19**, L675 (1986).